

Simulation of the process $e^+e^- \rightarrow W^+W^-$ with the heavy right-handed neutrino exchange at 1 TeV future lepton colliders

A. Drutskoy, E. Vasenin

P.N. Lebedev Physical Institute of the Russian Academy of Sciences, Moscow 119991, Russia

(Dated: November 20, 2024)

We study potential contribution of the heavy right-handed neutrino exchange in the process $e^+e^- \rightarrow W^+W^-$. This process is sensitive to heavy neutrinos with masses larger than \sqrt{s} . The Monte Carlo simulation of the studied process is performed assuming the Seesaw type-I model, where heavy right-handed neutrinos (heavy neutral leptons, HNL) are introduced in the leptonic sector. Within the Standard Model (SM), the process has a large cross section described by diagrams with s -channel Z/γ exchange and t -channel active neutrino exchange. Respectively, the t -channel right-handed neutrino exchange amplitude will interfere with these SM amplitudes. However, the angular distributions of the W boson production and decay are different for the right-handed neutrino and SM amplitudes. That can be used to evaluate potential HNL contribution using the extended likelihood method. The simulation of the $e^+e^- \rightarrow W^+W^-$ process is performed at the 1 TeV center-of-mass energy and polarisation $\mathcal{P}_{e^+e^-}$ of (20%, -80%), which is a standard option for the future linear e^+e^- collider ILC. Both W bosons are reconstructed from two hadronic jets. Simulation of the SM background processes is also done. The beam-induced backgrounds and the initial state radiation (ISR) effects are taken into account. The majority of background processes are effectively suppressed by the cuts on the invariant masses of two and four jets. Finally, we obtain upper limits on the mixing parameter $|V_{eN}|^2$ as a function of $M(N)$.

I. INTRODUCTION

We study the process $e^+e^- \rightarrow W^+W^-$ assuming contribution of the heavy right-handed neutrinos (Heavy Neutral Leptons, HNL, N) by t -channel exchange. Heavy right-handed neutrinos appear in many beyond the Standard Model (BSM) models to explain small masses of the active neutrinos [1–3]. HNL can generate Dirac masses of the active neutrinos with the Higgs mechanism [4–6]. However, this mechanism requires Yukawa coupling to be of $y_D \sim 10^{-12}$, which is difficult to explain. There are several studies within a generalized bottom-up Effective Field Theory, in which right-handed neutrinos naturally appear [7–10]. The most popular extensions of the lepton sector are within various Seesaw models, which are widely discussed today [11].

The process $l^-l^- \rightarrow W^-W^-$ ($l = e, \mu$) has been discussed in several papers [12–14], assuming opportunity for future same-sign electron or muon colliders. This process with t -channel HNL exchange is possible, if heavy neutrinos have a Majorana nature. In this process the lepton number violates by two units, therefore it has no backgrounds in the Standard Model. Using our experimental procedures we can well reproduce the results obtained in these papers. However, the same-sign lepton colliders are not considered as the possible option due to technical reasons. Therefore we study the similar process for the case of the opposite-sign beams.

In contrast to processes with direct HNL production [14–16], the $e^+e^- \rightarrow W^+W^-$ process is sensitive to contributions of HNLs with very large masses, $M(N) \gg \sqrt{s}$. Within the framework of the Seesaw type-I model, HNL masses can be large, therefore it is important to have experimental accessibility to the large HNL mass region. Since heavy right-handed neutrinos

have large mass, interference of the SM and HNL diagrams results in specific angular distributions in the W boson production and decays. We use these distributions within the extended likelihood method to evaluate the HNL contribution to the process and to obtain upper limits on the HNL mixing parameters. At the region $\sqrt{s} \sim 200 - 500$ GeV the SM $e^+e^- \rightarrow W^+W^-$ cross section is $\sim 1 - 2$ pb and the t -channel HNL exchange contributions are too small for experimental searches. In the paper [17] virtual HNL loop contributions were calculated and found to be also very small in this \sqrt{s} region.

Current experimental upper limits on the mixing parameters $|V_{lN}|$, $l = e, \mu, \tau$ have been discussed in [18, 19]. There are strict upper limits $|V_{eN}|^2 \lesssim 10^{-5}$ for the HNL masses less than the Z boson mass. However in the region $M(N) > 100$ GeV, the upper limits, mostly obtained by the LHC, are weak, $|V_{eN}|^2 \gtrsim 10^{-2}$ for $M_N < 1$ TeV and $|V_{eN}|^2 \gtrsim 1$ for $M_N > 1$ TeV. The latest results of searches for HNL performed by the LHC collaborations are presented in [20–24]. Future lepton colliders can significantly improve the upper limits in the large HNL mass region up to $\mathcal{O}(10^4 - 10^5)$ GeV.

We study the process within the Seesaw type-I model framework. Right-handed neutrinos are naturally introduced in the Seesaw type-I model. They transform as a singlet under SM gauge group and interact with the SM leptons through a Yukawa coupling. The Lagrangian of this interaction is given by

$$\mathcal{L}_N = -\overline{L}Y_\nu^D \tilde{H}N_R - \frac{1}{2}\overline{(N^c)}_L M_R N_R + \text{h.c.}, \quad (1)$$

where L and H are the left-handed lepton and Higgs doublets, respectively. Once H settles on the vacuum expectation value $\langle H \rangle = v_0/\sqrt{2}$, neutrinos acquire Dirac masses $m_D = Y_\nu^D v_0/\sqrt{2}$, and equation (1) transforms

into

$$\mathcal{L}_N \ni -\frac{1}{2}(\overline{\nu}_L m_D N_R + \overline{(N^c)}_L m_D^T (\nu^c)_R + \overline{(N^c)}_L M_R N_R) + \text{h.c.} \quad (2)$$

To obtain the mass eigenstates one introduces a unitary transformation

$$\begin{pmatrix} \nu \\ N^c \end{pmatrix}_L = U \begin{pmatrix} \nu_m \\ N_M^c \end{pmatrix}_L, \quad (3)$$

where m is the active neutrino mass, and M is the HNL mass. After unitary transformation, we obtain the neutrino mass matrix

$$U^\dagger \begin{pmatrix} 0 & m_D \\ m_D^T & M_R \end{pmatrix} U = \begin{pmatrix} m_\nu & 0 \\ 0 & M_N \end{pmatrix}, \quad (4)$$

In the limit of large M_R it results in the ratio between the masses of active and heavy neutrinos

$$m_\nu = -m_D M_R^{-1} m_D^T, \quad M_N \approx M_R. \quad (5)$$

From the latest equation it is seen, that large HNL masses favor small masses of active neutrinos, therefore it is important to test the large HNL mass region experimentally.

This study includes simulation and reconstruction of the process $e^+e^- \rightarrow W^+W^-$ to produce respective MC data samples. The following technical analysis of these samples is performed to estimate upper limits on the mixing parameters $|V_{eN}|^2$ as a function of the HNL masses. The generator Whizard version 3.1.5 [25, 26] is used to calculate matrix elements and to simulate phase space. The HeavyN model [27–30] is additionally included in the generator to calculate the amplitude with the HNL exchange. Pythia6 [31] is used for hadronisation and W boson decay simulation and hadronisation. The Delphes [32] package is used for fast detector simulation and event reconstruction. Finally, the analysis of reconstructed events is performed by the ROOT package [33].

II. EXPERIMENTAL PROCEDURES

A. Monte Carlo simulation and event reconstruction

The signal process $e^+e^- \rightarrow W^+W^-$ is described by the diagrams with the s -channel Z/γ exchange and by the diagrams with the t -channel neutrino (light or heavy) exchange as shown in Fig. 1(a,b). For simplicity, we assumed that only one heavy neutrino is present.

At the first step, the Whizard generator is used to calculate the matrix elements and to perform phase space Monte Carlo simulation. The matrix elements are calculated for every diagram describing the process. The amplitudes are then summed up taking into account the interference between the diagrams. The event generation is performed at the center-of-mass energy $\sqrt{s} = 1$ TeV and

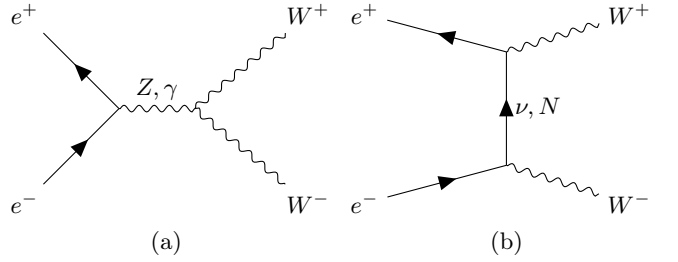


FIG. 1. The $e^+e^- \rightarrow W^+W^-$ diagrams with s -channel (a) and with t -channel (b) exchanges

the polarisation $\mathcal{P}_{e^+e^-}$ of (20%, -80%), which is a standard option for the future International Linear Collider (ILC) [34]. The ISR effects are taken into account using Whizard in-built package. Beam-induced backgrounds simulated using the CIRCE2 package are added to the $e^+e^- \rightarrow W^+W^-$ events. The subsequent decays of the W bosons into hadronic jets and following hadronisation is performed by PYTHIA6. PYTHIA6 reproduces correct angular distributions for hadronic jets from W boson decays.

For a process described by several diagrams, Whizard allows to calculate a single matrix element for a particular diagram or a set of diagrams. We calculate the cross sections corresponding to the HNL diagram only to see the behavior of the cross section as a function of the HNL mass. The cross sections are calculated for $|V_{eN}|^2 = 0.0021$ and different beam polarisation options, as shown in Fig. 2. The contribution of the HNL diagram becomes smaller at the large $M(N)$ region, respectively the upper limits on the mixing parameters become weaker with the HNL mass increase. The largest cross section is obtained for the beam polarisation $\mathcal{P}_{e^+e^-}$ of (20%, -80%).

Further detector simulation and event reconstruction are performed by the Delphes package. A preinstalled detector card is required in Delphes for the fast detector simulation. We use the "ILCgen" card that performs simulation corresponding to the ILC detector presented in the technical design report [35]. This card describes responses of different subdetectors and provides realistic resolutions in the energy, momentum and other physical parameters.

We select events with four jets and no leptons in the final state. To reconstruct jets in the hadronic calorimeter, we use Valencia clustering algorithm [36] with the default parameters $R = 1.0$, $\beta = 1.0$ and $\gamma = 0.5$. If a W boson has a large momentum, the two produced hadronic jets overlap and, by default, are considered as one "fat-jet" by the jet clustering algorithm. However, we force the algorithm to find exactly four jets, and therefore do not lose events with "fat-jets" which are forced to be split into two jets. We test all jet pair combinations and choose the W candidates with the mass closest to the nominal mass of the W boson. In case of "fat-jets", the individual jet parameters can be somewhat incorrect, but the combination of the two jets accurately reproduces the W

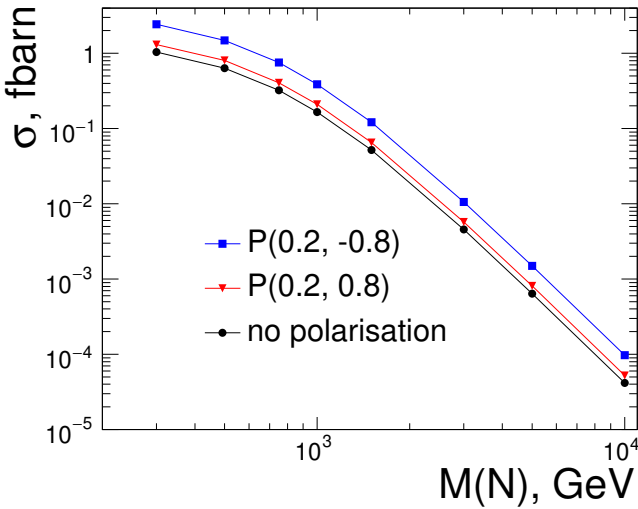


FIG. 2. The cross sections of the $e^+e^- \rightarrow W^+W^-$ process with only HNL diagram taken into account for different beam polarisation options are shown. Blue squares correspond to $\mathcal{P}_{e^+e^-}$ of (20%, -80%), red triangles to $\mathcal{P}_{e^+e^-}$ of (20%, 80%) and black circles to unpolarised beams.

boson candidate parameters.

B. Preselections

The initial preselections require the transverse momenta and pseudorapidities of the hadronic jets to be within the detector acceptance:

$$P_t(j) > 20 \text{ GeV}, \quad |\eta(j)| < 2.17, \quad (6)$$

As the effects induced by the exchange of a right-handed neutrino are enhanced in the central region, both W bosons are required to be central

$$|\cos \theta| < 0.7, \quad (7)$$

where θ is an angle between the direction of the W boson and the beam.

These preselections are applied at the generator level and significantly reduce the sizes of the studied event samples.

C. Backgrounds and cuts

The studied backgrounds must have four jets and no leptons in the final state. In addition, the background process $e^+e^- \rightarrow q\bar{q}$ could produce two "fat-jets" reconstructed as four jets, therefore it also has to be considered. The same procedure with the same parameters is used to simulate and reconstruct background events as it is done for the signal events. The following background processes are generated, which are expected to be non-negligible in this study:

- a) $e^+e^- \rightarrow W^+W^-$ (with s -channel Z/γ exchange and t -channel active neutrino exchange)
- b) $e^+e^- \rightarrow W^+W^-\nu_e\bar{\nu}_e$
- c) $e^+e^- \rightarrow q\bar{q}$
- d) $e^+e^- \rightarrow ZZ$

To distinguish between the signal and the background events, we use the following variables:

- a) $M(jj)$ - the mass of a jet pair corresponding to the W boson candidate
- b) $M(4j)$ - the mass of four jets
- c) $\sum p_x$ and $\sum p_y$ - the sum of the p_x or p_y momentum components of all reconstructed final state objects in the event

To suppress most of the backgrounds except the process $e^+e^- \rightarrow W^+W^-$ the following cuts are applied:

$$70 \text{ GeV} < M(jj) < 90 \text{ GeV}, \quad (8)$$

$$M(4j) > 600 \text{ GeV}, \quad (9)$$

$$\left| \sum p_x \right| < 100 \text{ GeV}, \quad \left| \sum p_y \right| < 100 \text{ GeV}. \quad (10)$$

The $M(jj)$ and $M(4j)$ distributions for the signal and background events are shown in Fig. 3 and Fig. 4, respectively. The cuts on the $M(4j)$ and $\sum p_x/p_y$ variables are used to remove most of the backgrounds with energetic unregistered particles in the final state. The cut on $M(jj)$ is used to suppress backgrounds where the two chosen hadronic jets do not correspond to a W boson. It is seen in Fig. 3 that this cut effectively suppresses most of the background events. The numbers of events in the generated samples before and after applied cuts are shown in Table I. The HNL contribution is calculated for $|V_{eN}|^2 = 0.01$, $M(N) = 300$ GeV. Also shown in Table I is the SM contribution to $e^+e^- \rightarrow W^+W^-$. The event yields are normalized to the integrated luminosity of 1 ab^{-1} .

TABLE I. Numbers of events in the studied samples for $\mathcal{L}_{\text{int}} = 1 \text{ ab}^{-1}$, $\sqrt{s} = 1 \text{ TeV}$, $\mathcal{P}_{e^+e^-} = (20\%, -80\%)$, and preselections described above. We assume $|V_{eN}|^2 = 0.01$, $M(N) = 300$ GeV for (SM+HNL) process.

Process	Events after preselections	Events after all cuts	$\varepsilon, \%$
$e^+e^- \rightarrow$			
W^+W^- (SM+HNL)	661674	531906	80.3
W^+W^- (SM)	525524	417889	79.5
$q\bar{q}$	716317	5005	0.7
ZZ	29419	1175	4.0
$W^+W^-\nu_e\bar{\nu}_e$	6041	328	0.5

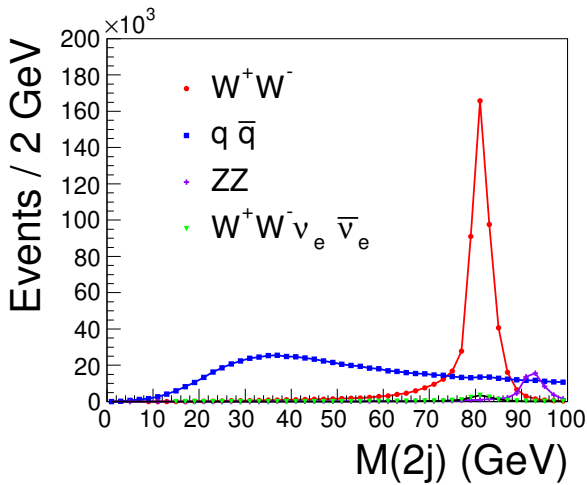


FIG. 3. The $M(jj)$ distributions for the processes $e^+e^- \rightarrow W^+W^-$ (red circles), $e^+e^- \rightarrow q\bar{q}$ (blue squares), $e^+e^- \rightarrow ZZ$ (purple crosses), and $e^+e^- \rightarrow W^+W^-\nu_e\bar{\nu}_e$ (green triangles).

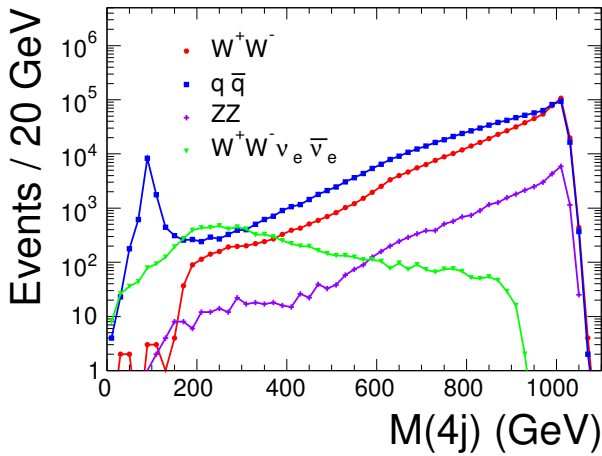


FIG. 4. The $M(4j)$ distributions for the processes $e^+e^- \rightarrow W^+W^-$ (red circles), $e^+e^- \rightarrow q\bar{q}$ (blue squares), $e^+e^- \rightarrow ZZ$ (purple crosses), and $e^+e^- \rightarrow W^+W^-\nu_e\bar{\nu}_e$ (green triangles).

D. Angular distributions

The $e^+e^- \rightarrow W^+W^-$ process is described by five angles $\theta, \theta_1, \theta_2, \phi_1, \phi_2$ as shown in Fig. 5. Three out of them, $\theta, \theta_1, \theta_2$ are used to distinguish the SM+HNL contribution from the SM-only contribution. The production angle θ is the angle between the W boson direction and the e^- beam direction in the laboratory system. The decay angles θ_1 and θ_2 are the angles between the jet direction and the e^- beam direction in the W boson rest frame. θ_1 is the decay angle of W boson with the larger angle with the e^- beam direction and θ_2 is the decay angle of

the second W boson. Because of the large mass of heavy neutrino, the distributions of the variables $\theta, \theta_1, \theta_2$ for the SM and HNL contributions are different. Therefore we can use these distributions to estimate the significance of the HNL contribution. The distributions of angles ϕ_1 and ϕ_2 between the production and decay planes for the signal and background events are very similar and are not used in this study.

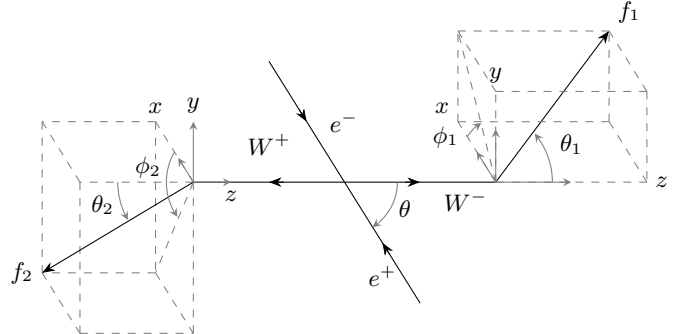


FIG. 5. The angles used in the analysis of the process $e^+e^- \rightarrow W^+W^-$ with the subsequent W boson decay into two hadronic jets

The event simulation is performed for three different cases: SM-only, HNL-only, and SM+HNL. The simulation of the $e^+e^- \rightarrow W^+W^-$ process with only the HNL diagram included at the generator level is performed to demonstrate the shapes of the respective angular distributions. The distributions of $\cos\theta$ and $\cos\theta_{1,2}$ are shown in Fig. 6 and Fig. 7, respectively. The figures demonstrate the difference in the shapes of the angular distributions for the SM and HNL diagrams. In the simulation the parameters $|V_{eN}|^2 = 0.0225$ and $M(N) = 500$ GeV are used. These parameters provide larger signal than the parameters used in Table I to make signal more visible.

III. ANALYSIS

To determine the upper limits on the mixing parameter we use the extended likelihood method. The null hypothesis corresponds to the Standard Model case without the HNL contribution. The non-null hypothesis includes a non-zero HNL amplitude interfering with the SM amplitudes. The significance of the HNL contribution is calculated as

$$S = -2 \ln \frac{\mathcal{L}_0}{\mathcal{L}_1}, \quad (11)$$

where \mathcal{L}_0 is the likelihood function for the null hypothesis, and \mathcal{L}_1 is the likelihood function for the non-null hypothesis. The values of the likelihood functions for a given data sample can be calculated from the following expression

$$\mathcal{L}_{0,1} = P(N|N_{0,1}) \cdot \prod_i f_{0,1}(x^i), \quad (12)$$

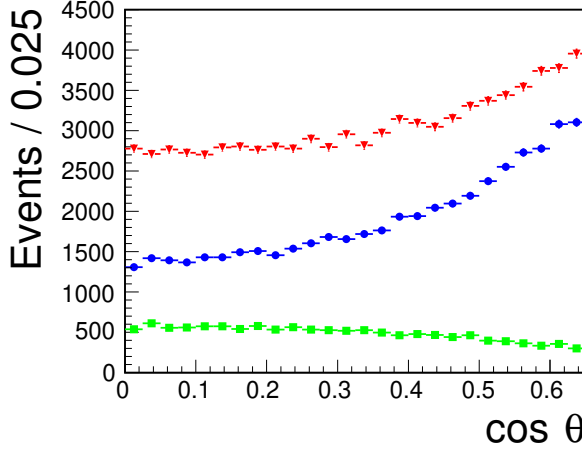


FIG. 6. The W production angular distributions for SM-only $e^+e^- \rightarrow W^+W^-$ (blue circles), HNL-only $e^+e^- \rightarrow W^+W^-$ (green squares), and the SM+HNL interference (red triangles).

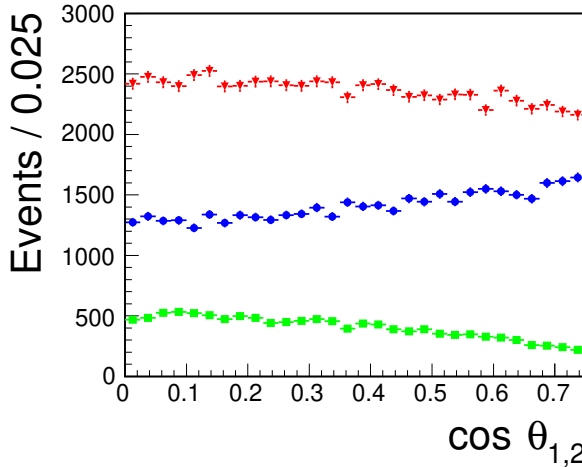


FIG. 7. The W decay angular distributions for SM-only $e^+e^- \rightarrow W^+W^-$ (blue circles), HNL-only $e^+e^- \rightarrow W^+W^-$ (green squares), and the SM+HNL interference (red triangles).

where N is the number of events in the data sample, $N_{0,1}$ is the mean number of events for the respective hypothesis, and $P(N|N_{0,1})$ is the Poisson function. The product is taken over all events in the data sample. The function $f_{0,1}(x)$ is the probability density function of the studied variables $x = (\theta, \theta_1, \theta_2)$.

It is seen from equation (12) that the likelihoods are sensitive to the two factors. First, the event number in the data sample depends on HNL contribution, and it is taken into account by the Poisson term. Second, the interference between the HNL and SM diagrams changes

the distribution shape, and that is accounted for by the product term in the likelihood function.

To determine the probability density functions, two training data samples are generated. $f_0(x)$ are determined from the data sample produced without HeavyN model included in the generator. The second data sample, used to evaluate $f_1(x)$ is generated with the HeavyN model included. The mixing parameter and the HNL mass are chosen in the studied region. After producing the data samples we apply the cuts described above and study the three-dimensional distributions of the $\theta, \theta_1, \theta_2$ angles. No correlations between them are found, so the three-dimensional probability density function has been chosen as a product of the one-dimensional probability density functions

$$f(x^i) = f(\theta^i) \cdot f(\theta_1^i) \cdot f(\theta_2^i), \quad (13)$$

One-dimensional p.d.f.'s are defined as follows

$$f(\theta) = a(\cos \theta)^4 + b(\cos \theta)^2 + c, \quad (14)$$

$$f(\theta_{1,2}) = a_{1,2}(\cos \theta_{1,2})^2 + b_{1,2}, \quad (15)$$

where $a, a_{1,2}, b, b_{1,2}, c$ are the free parameters of the fit.

To improve the fit sensitivity to the HNL contribution, the fit is constrained to the regions $0.0 \leq \cos \theta \leq 0.6$ and $0.0 \leq \cos \theta_{1,2} \leq 0.7$. Therefore we fit $\cos \theta$ distributions in the $[0.0, 0.6]$ range and the $\cos \theta_{1,2}$ distributions in the $[0.0, 0.7]$ range. The distributions in these regions are smooth and well described by the functions above. Finally, we perform a three-dimensional fit of the $\cos \theta, \cos \theta_1, \cos \theta_2$ distributions using RooFit package [37].

One more test data sample is generated to determine the likelihood functions and estimate the significance of the HNL contribution for the chosen mixing parameters and masses. We fix a specific $M(N)$ value and perform the fit for different values of the mixing parameter to obtain the significance corresponding to the 90 % upper limit. To determine the upper limit as a function of $M(N)$, the same procedure is repeated for all tested $M(N)$ values. The results are shown in Fig. 8.

As it is seen in Fig. 8, the obtained upper limits are significantly better than those obtained at LHC [18] in the region of $300 \text{ GeV} < M(N) < 1 \text{ TeV}$. Moreover our results are sensitive to the HNL mass region up to 10^4 GeV , where the upper limit reaches the value $|V_{eN}|^2 \sim 1$.

IV. CONCLUSIONS

We studied the potential Heavy Neutral Lepton contribution to the process $e^+e^- \rightarrow W^+W^-$ within the framework of the Seesaw type-I model. The MC simulation and reconstruction of the signal and background processes is performed for future e^+e^- colliders at 1 TeV. The upper limits on the mixing parameter $|V_{eN}|^2$ are obtained as a

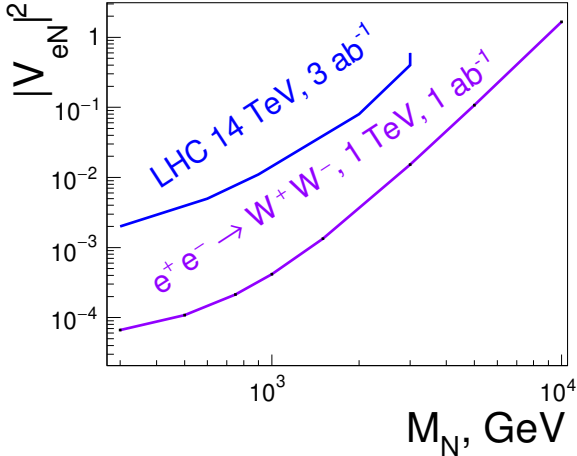


FIG. 8. The upper limits on the mixing parameter $|V_{eN}|^2$ as a function of $M(N)$ (purple line). Our results are compared to the LHC projection for 3 ab^{-1} [29] (blue line).

function of HNL mass $M(N)$. An experimental study of the $e^+e^- \rightarrow WW$ process can significantly improve the current upper limits in the region of HNL masses larger than \sqrt{s} and effectively test specific Seesaw type I models. However, the search for direct HNL production can give better upper limits in the region $M(N) < \sqrt{s}$ [15].

It has to be mentioned, that there are excellent prospects for the HNL searches in the $e^+e^- \rightarrow W^+W^-$ or $\mu^+\mu^- \rightarrow W^+W^-$ processes at very high collision energies. With increasing collision energies, the cross section of the SM process $e^+e^- \rightarrow W^+W^-$ fastly decreases, whereas the HNL induced cross section increases. Therefore, future lepton colliders with the $\sqrt{s} = 3 \text{ TeV}$ and $\sqrt{s} = 10 \text{ TeV}$ center of mass energies can provide strict upper limits on the mixing parameters $|V_{lN}|^2$. We plan to conduct respective calculations in the future.

[1] Y. Fukuda *et al.* (Super-Kamiokande Collaboration), *Phys. Rev. Lett.* **81**, 1562 (1998).

[2] Ahmad, Q. R. *et al.* (SNO Collaboration), *Phys. Rev. Lett.* **89**, 011301 (2002).

[3] K. Eguchi *et al.* (KamLAND Collaboration), *Phys. Rev. Lett.* **90**, 021802 (2003).

[4] C.-Y. Yao and G.-J. Ding, *Phys. Rev. D* **96**, 095004 (2017).

[5] S. Kanemura, T. Nabeshima and H. Sugiyama, *Phys. Lett. B* **703**, 66 (2011).

[6] J. Sudip, P. K. Vishnu and S. Shaikh, *JCAP* **2020**, 018 (2020).

[7] S. Bhattacharya and J. Wudka, *Phys. Rev. D* **94**, 055022 (2016).

[8] Y. Liao and X.-D. Ma, *Phys. Rev. D* **96**, 015012 (2017).

[9] H.-L. Li, Z. Ren, M.-L. Xiao *et al.*, *JHEP* **2021**, 3 (2021).

[10] F. del Águila, S. Bar-Shalom, A. Soni and J. Wudka, *Phys. Lett. B* **670**, 399 (2009).

[11] Y. Cai, T. Han, T. Li and R. Ruiz, *Front. Phys.* **6**, (2018).

[12] T. Asaka and T. Tsuyuki, *Phys. Rev. D* **92**, 094012 (2015).

[13] R. Jiang, T. Yang, S. Qian, Y. Ban, J. Li, Z. You and Q. Li, *Phys. Rev. D* **109**, 035020 (2024).

[14] S. Banerjee, P.S. Bhupal Dev, A. Ibarra, T. Mandal and M. Mitra, *Phys. Rev. D* **92**, 075002 (2015).

[15] K. Mękała, J. Reuter and A. F. Żarnecki, *JHEP* **2022**, 10 (2022).

[16] E. Antonov, A. Drutskoy and M. Dubinin, *Jetp Lett.* **118**, 461 (2023).

[17] K.-P.O. Diener, B. A. Kniehl and A. Pilaftsis, *Phys. Rev. D* **57**, 2771 (1998).

[18] A. M. Abdullahi *et al.*, *J. Phys. G* **50**, 020501 (2023).

[19] P.D. Bolton, F.F. Deppisch and P.B. Dev, *J. High Energ. Phys.* **2020**, 170 (2020).

[20] A. Hayrapetyan *et al.* (CMS Collaboration), *JHEP* **2024**, 105 (2024).

[21] A. Hayrapetyan *et al.* (CMS Collaboration), *arXiv:2407.10717 [hep-ex]*.

[22] A. Hayrapetyan *et al.* (CMS Collaboration), *JHEP* **2024**, 123 (2024).

[23] A. Hayrapetyan *et al.* (CMS Collaboration), *Phys. Rev. D* **110**, 012004 (2024).

[24] ATLAS collaboration, *arXiv:2408.05000 [hep-ex]*.

[25] M. Moretti, T. Ohl and J. Reuter, *arXiv:hep-ph/0102195*.

[26] W. Kilian, T. Ohl and J. Reuter, *Eur. Phys. J. C* **71**, 1742 (2011).

[27] D. Alva, T. Han and R. Ruiz, *JHEP* **2015**, 072 (2015).

[28] C. Degrande, O. Mattelaer, R. Ruiz and J. Turner, *Phys. Rev. D* **94**, 053002 (2016).

[29] S. Pascoli, R. Ruiz and C. Weiland, *JHEP* **2019**, 049 (2019).

[30] A. Atre, T. Han, S. Pascoli and B. Zhang, *JHEP* **2009**, 030 (2009).

[31] T. Sjöstrand, S. Mrenna and P. Skands, *JHEP* **05**, 026 (2006).

[32] J. de Favereau, C. Delaere *et al.* (The DELPHES 3 collaboration), *JHEP* **2014**, 057 (2014).

[33] R. Brun *et al.*, *root-project/root*: v6.18/02.

[34] C. Adolphsen *et al.*, *arXiv:1306.6353 [physics.acc-ph]*.

[35] T. Behnke, J.E. Brau, B. Foster, J. Fuster, M. Harrison, J.M. Paterson, M. Peskin, M. Stanitzki, N. Walker and H. Yamamoto, *arXiv:1306.6329 [physics.ins-det]*.

[36] M. Boronat, J. Fuster, I. Garcia *et al.*, *Eur. Phys. J. C* **78**, 144 (2018).

[37] V. Wouter and D. Kirkby, *arXiv:physics/0306116 [physics.data-an]*.